Information Sciences 642 (2023) 119129

Contents lists available at ScienceDirect

Information Sciences

journal homepage: www.elsevier.com/locate/ins

Fuzzy-VGG: A fast deep learning method for predicting the staging of Alzheimer's disease based on brain MRI

Zhaomin Yao [a,b], Wenxin Mao [c], Yizhe Yuan [c], Zhenning Shi [c], Gancheng Zhu [d], Wenwen Zhang [a,b], Zhiguo Wang [a,b,*], Guoxu Zhang [a,b,*]

[a] Department of Nuclear Medicine, General Hospital of Northern Theater Command, Shenyang, Liaoning 110016, China
[b] College of Medicine and Biological Information Engineering, Northeastern University, Shenyang, Liaoning 110167, China
[c] College of Computer Science and Technology, Jilin University, Changchun, Jilin 130012, China
[d] Center for Psychological Sciences, Zhejiang University, Hangzhou, Zhejiang 310027, China

ARTICLE INFO

Keywords:
Alzheimer's disease
Brain MRI
Fuzzy
Cutout
Stage prediction

ABSTRACT

Alzheimer's disease, a primary degenerative encephalopathy, predominantly affects elderly and pre-elderly individuals and is characterized by persistent anxiety-like brain activity. Despite magnetic resonance imaging emerging as a crucial tool for examining brain tissues and diagnosing Alzheimer's disease, most existing studies solely focus on detecting the disease's presence, neglecting its staging. Furthermore, these methods generally focus on the improvement of an algorithm architecture rather than on improving the quality of medical images. This paper aims to address this limitation by presenting a novel method, Fuzzy-VGG. With this approach, the image pixels are reordered based on their gray levels using fuzzy theory, placing a high priority on the most significant local information in each pixel. Following this, a VGG-based primary framework is employed to train the datasets, and a two-stage cutout strategy is used to augment the dataset and enhance training results. The results demonstrate substantial improvements in classification performance and accelerated model convergence. The primary novelties and contributions of this work encompass: 1) a focus on local key areas to expedite training and enhance results, 2) the utilization of a two-stage cutout data enhancement strategy tailored to medical images' characteristics, and 3) seamless integration with blockchain technology to facilitate scalability and continuous model improvement.

1. Introduction

Alzheimer's disease (AD) is an insidious and progressive neurodegenerative disorder. It refers to a group of neurological disorders characterized by memory loss, cognitive impairment, and disability in activities of daily living [1,2]. This disease is the most common type of dementia among elderly patients, accounting for approximately 50–60% of elderly patients with dementia [3]. Additionally, aging is associated with an increase in the incidence and severity of it [4,5]. Alzheimer's disease diagnosis in primary care can be challenging; many of the early symptoms are non-specific and can be difficult to differentiate from the symptoms of common normal aging. Meanwhile, it may be misdiagnosed as other forms of dementia due to similar clinical and pathological features [6,7]. In brief,

* Corresponding authors at: Department of Nuclear Medicine, General Hospital of Northern Theater Command, Shenyang, Liaoning 110016, China.
E-mail addresses: wangzhiguo5778@163.com (Z. Wang), zhangguoxu_502@163.com (G. Zhang).

https://doi.org/10.1016/j.ins.2023.119129
Received 28 December 2022; Received in revised form 4 May 2023; Accepted 7 May 2023
Available online 12 May 2023

there are limitations to conventional diagnosis methods, such as determining whether memory loss in early Alzheimer's patients is due to Alzheimer's disease. In addition, existing diagnostic tools cannot identify early pathological changes in the brain. The result is that a large number of Alzheimer's patients cannot be identified in their early stages. Therefore, prompt, accurate staging of diagnosed Alzheimer's disease is of vital importance to the care and treatment of these patients.

Brain magnetic resonance imaging (MRI) is a powerful, noninvasive imaging tool able to help accurately detect or diagnose Alzheimer's Disease by providing anatomical, functional, and metabolic MRI information [8,9]. Due to its imaging mechanism, it is highly sensitive to brain contraction and can be used to construct 3D brain tissue images at high resolution [10,11]. Moreover, structural MRI measurements of atrophy are important biomarkers to track disease progression in Alzheimer's disease (AD) [12–15]. Thus, following the rapid development of artificial intelligence technology, widespread use of computer-aided diagnosis in Alzheimer's disease based on MRI images.

Deep learning has made great strides in medical image diagnosis over the last decade. Several deep neural networks have been modified and applied for detecting Alzheimer's disease in recent years. An mRMR-based hybrid CNN was developed to classify Alzheimer's disease in brain images using machine learning architectures [16]. Utilized the AlexNet framework to retrieve salient features of MRI for Alzheimer's disease diagnosis [17]. To diagnose Alzheimer's disease (AD), a U-net-style diagnostic model combining 3D T1-weighted magnetic resonance images (MRI) was proposed with deep supervision [18]. Also, many scientists have attempted to diagnose Alzheimer's disease using a variety of data-fusion methods. Local and global information of the brain was extracted from the landmark-based deep multi-instance learning platform (LDMIL) for AD-related brain disease diagnosis [19]. A new method for diagnosing Alzheimer's disease using MRI images combined with deep learning and image processing is proposed [20]. Early Alzheimer's disease can be diagnosed with hierarchical transfer learning and tissue segmentation of brain images [21]. In addition, there have been numerous innovative attempts in the field of neural networks. An AlzNet learning network was established by two-dimensional slices collected from MRI scans to train convolutional neural networks [22]. DEMNET was developed by using convolutional neural networks, synthetic minority oversampling techniques to eliminate class imbalances, reducing model parameters and calculation costs [20]. A REVGAN model was proposed to reconstruct the missing data to use multi-modal complementary information, and a 3D convolutional neural network classification model was then proposed to diagnose AD based on multi-modal inputs [23].

As with distributed ledgers, blockchain technology is a technology for building Internet databases that facilitate decentralization, openness, and transparency by allowing anyone to contribute to database records. Biometric data, such as genetic information or electronic medical record, can be stored securely on blockchains, and then accessed through a private key to create a "wallet" similar to DNA information [24]. As a result, medical units can automatically retrieve relevant data from the entire network based on their authorization level, thereby aiding in the diagnosis of disease and the development of new drugs.

1.1. Contributions and novelties

Even though these state-of-the-art methods have achieved good results, their primary concern is to determine if this patient has AD, instead of focusing on AD staging. In addition, these methods usually only focus on the improvement of a specific algorithm architecture and do not consider improving the quality of medical images. To address the above two pivotal questions, we propose a deep learning method to analyze the staging of Alzheimer's disease on brain MRI images. The main contributions and novelties of this work are listed as follows.

1. Focus on local key areas. Usually, medical images contain interest regions and background regions. Detailed diagnostic information in interest regions can provide a reliable basis for treatment and research in pathology. In this method, the fuzzy theory emphasizes local key information, which speeds up training, reduces training time, and improves training results.
2. Enhancement of medical images based on their characteristics. Medical images with the same posture have a very high similarity due to the high similarity of human tissue. As a result, a two-stage cutout data enhancement strategy is employed to address this issue. [25]. Through this technique, the network can better utilize the full context of the image, rather than relying purely on a small set of specific visual features. At the same time, this technique is noise-free.
3. Easy to integrate with blockchain technology. In the blockchain, the public chain is open, tamper-proof, traceable, cross-regional, and decentralized. Additionally, the proposed model is scalable and mobile. When new data on public chains arrive, the model can be easily improved.

The following of this article was organized as the section "Materials and Methods" described the details of the datasets and the overview of the methods, the experimental results were described and discussed in the section "Results and Discussions", and the section "Conclusions" was the concluding remarks.

2. Materials and methods

2.1. Datasets

Two kinds of brain MRI imaging datasets are used in this study, including the Kaggle Alzheimer's classification dataset (KACD) [26] and the Recognition of Alzheimer's Disease dataset (ROAD) [27]. The KACD dataset comprises four different degrees of Alzheimer's disease images, which are Non-Demented, Very Mild Demented, Mildly Demented, and Moderately Demented. The other ROAD

Pseudocode of Fuzzy C-Means Image Processing

Input. The images S. The parameter ε is Error threshold and the parameter $Max\_Iteration$ i the maximum number of iterations

Output. New images with adjusting pixel information

Step 1. Load the image, set ε and $Max\_Iteration$, initialize all pixel point values and randomly select the center point of each cluster, initialize the fuzzy value P_i corresponding to the related pixel i and calculate the cluster index

While $Max\_Iteration$ is not reach do:

Step 2. Initialize $U = [u_{ik}]$ matrix, U^0

Step 3. At l-step: calculate the centers vectors $V^l = [V_k]$ with U^l

$$V_k = \frac{\sum_{i=1}^{n} \mu_{ik}^m P_i}{\sum_{i=1}^{n} \mu_{ik}^m P_i}$$

Step 4. Update U^l and U^{l+1}

$$\mu_{ik} = \frac{1}{\sum_{l=1}^{c} (\frac{|P_i - V_k|}{|P_i - V_l|})^{\frac{2}{m-1}}}$$

Step 5. Test the data and return the segmented images with the best overall segmentation performance. If $\|U^{l+1} - U^l\| < \varepsilon$ then break, else back to **Step 3**.

End while

Step 6. Generate the new image according to the P

Fig. 1. Pseudocode of Fuzzy C-Means Image Processing.

dataset contains three categories, Non-Demented, Mildly Demented, and Alzheimer's disease. Meanwhile, KACD has 9109 2D MRI samples and ROAD has 749 3D MRI samples (All of the 3D data presented here are 2D slices). Full details of these datasets are described in the Supplementary Table S1. The sample images can be seen in Supplementary Figure. S1 and S2.

2.2. Fuzzy C-Means

Common neurodegenerative diseases are associated with progressive and localized cortical atrophy with a well-defined anatomical distribution. In order to emphasize the information regarding progressive and localized cortical atrophy with a well-defined anatomical distribution in brain MRI images, the fuzzy C-Means algorithm is applied. By rearranging pixels and adjusting gray levels, this preprocessing technique effectively highlights pertinent information in the dataset. [28,29].

Fuzzy C-Means (FCM) integrates the essence of fuzzy theory. It provides better clustering results than traditional K-Means, as it uses clustering to modify the pixels of the graph, allowing the lesion area's image information to be implicitly labeled and the model to be found more expeditiously. In most cases, you cannot divide objects in a dataset into very independent clusters. Assigning objects to specific clusters are very strict and can go wrong. Therefore, each object-cluster pair is assigned a weight indicating how well the object matches the cluster. Probabilistic-based methods can also provide such weights, but determining a suitable statistical model can be difficult. The best option here is Fuzzy C-Means, which has natural and non-host properties.

As shown in Equation (1), the core target of this algorithm is to minimize the objective function.

$$J_m = \sum_{i=1}^{n} \sum_{k=1}^{c} \mu_{ik}^m \|P_i - V_k\|^2 \tag{1}$$

In this formula, m stands for the number of clusters, i, and k stands for the class label. u_{ik} represents the membership degree of sample P_i belonging to class k. V_k is the center of class k. $\|*\|$ is an arbitrary measure of distance. Fuzzy C-Means is a continuous iterative calculation process of membership u_{ik} and cluster center V_k until they reach the optimum. For a single sample P_i. The sum of its membership degrees for each cluster is 1. The pseudo code of fuzzy C-Means image processing detailed description in Fig. 1.

2.3. Two-stage cutout

The cutout strategy is used in this step to enhance the dataset [30,31], that is, randomly cut out a square area in the image, fill in zero in the original image and then perform two-stage model training. Additionally, cutout and training are conducted simultaneously. In the first stage, the cutout method involves randomly cutting out a square area of a previously determined size (which can be set by the user) from the original image, and filling it with 0 pixels, leaving empty space in the original picture. Alternatively, the zero-filled area may be an irregular shape; however, since the two effects are similar, it is deemed more convenient to select the square shape. Initially, the data set image is reduced to 112×112, and the image is removed. In the subsequent training, the processed data is utilized to select the model that demonstrates the best classification performance. In the second stage, the size of the data set is restored to 224×224, and the image is still cut out. After the newly processed data set has been processed, continue to train the best model which was selected in the first step. A final model is selected based on its classification performance during training. This model will be utilized for migration learning for subsequent classification. Cutout is designed to encourage the model to pay greater attention to the global information in the image, and two-stage processing reinforces this point even more. The model will be able to understand the global information better after two different size cutouts have been made from the image. In addition, the model's processing of two common sizes also provides universality and robustness for images of different sizes when discriminating between them.

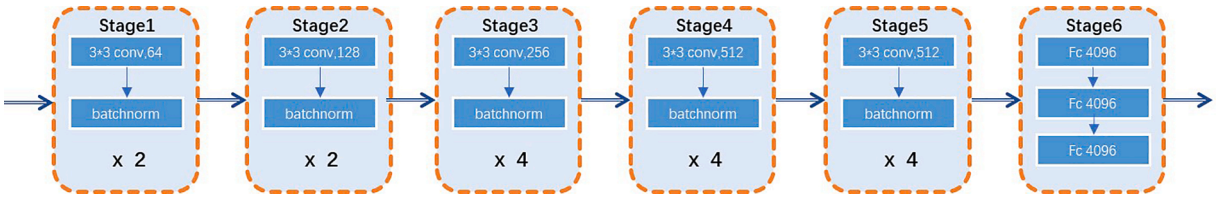

Fig. 2. The framework of the method.

2.4. Model construction

There are three components in the framework implemented in this study, which include the backbone, neck, and head. The images will be resized to match the original network and then the model will be inputted. This framework relies on VGG_BN [32,33] as its backbone, as illustrated in Fig. 2. The convolution block is composed of a convolution layer and a batch norm layer, collectively referred to as the convolution block in this context. There are six stages in VGG_BN. Stages 1–5 are stacks of multiple convolution blocks. Convolution layers have different core sizes and stacking times, as well as different stacking times for Conv blocks. In this instance, the core size is 64,128,256,512,512, and the stacking times are 2, 2, 4, 4, 4. Three full connection layers with 4086 units make up the last stage. The results are then output by the final full connection layer. In terms of learning more complex patterns, stacked small convolutional kernels offer a superior solution to large convolutional kernels for a given receptive field. Multi-layer nonlinear layers can ensure the depth of the network and are relatively inexpensive. BN layers can limit the number of inputs to a range and then convert the data back to normal distributions. The AdaptiveConcatPool2d function, which forms the neck of the framework, performs global pooling based on the feature map extracted from the backbone network, that is, a feature map $N \times N \times C$ becomes $1 \times 1 \times 2C$ by using max pooling and average pooling. This function is primarily beneficial in three ways: saving parameters, adjusting the size of the input adaptively, and introducing regularization to express the goal abstractly.

The Cross Entropy Loss is the head of the framework. The goal is for the predicted probabilities to be as close to the original distribution as possible. Cross entropy helps minimize the difference between predicted and actual probabilities. As a result, it is a suitable loss function to use in the study. Following is a description of the function:

$$Loss(x, class) = -\log\left(\frac{\exp(x[class])}{\sum_j \exp(x[j])}\right) = -x[class] + \log\left(\sum_j \exp(x[j])\right) \tag{2}$$

Where x represents the probability that the point belongs to different categories, and *class* represents the category to which the point belongs.

2.5. Performance metrics

The prediction performances of the six commonly used classification methods are assessed in this study, which are ACC, SN (sensitivity), SP (specificity), PR (precision), F1-SCORE, and MCC. The equations of these metrics are listed as follows:

$$\begin{aligned} Acc &= \frac{TP + TN}{TP + FP + TN + FN} \\ SN &= \frac{TP}{TP + FN} \\ SP &= \frac{TP}{TN + FP} \\ PR &= \frac{TP}{TP + FP} \\ F1 - Score &= \frac{2 \times PR \times SE}{PR + SE} \\ MCC &= \frac{TP \times TN - FP \times FN}{\sqrt{(TP + FP)(TP + FN)(TN + FP)(TN + FN)}} \end{aligned} \tag{3}$$

Where TP, TN, FP, and FN denote true positive, true negative, true positive, and false negative predictions, respectively.

3. Results and Discussions

3.1. Result of images with fuzzy

In Fig. 3, the two images on the left are the original image without fuzzy-C-means and the gray distribution map of the image. The image on the right is the image after fuzzy-C-means processing and its gray distribution. The gray distribution image is modified by

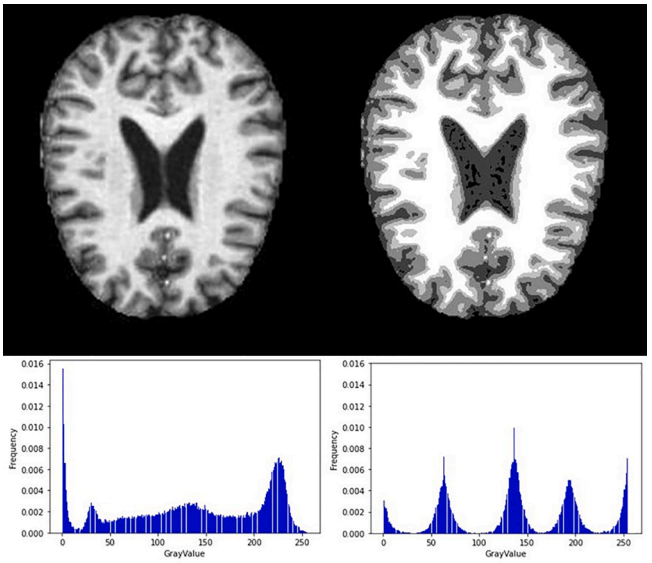

Fig. 3. Sample Images Before and After Fuzzy C-Means and Their Gray Distribution.

Table 1
Classification results with different enhancement modules.

Dataset	Type	Modules	ACC	SN	SP	PR	F1 Score	MCC
KACD	Binary	None	0.9605	0.9268	0.9702	0.9426	0.9329	0.9056
		Fuzzy	0.9492	0.8906	0.9627	0.9222	0.9030	0.8692
		Two-stage Cutout	0.9932	0.9877	0.9948	0.9901	0.9888	0.9839
		Above two	0.9898	0.9772	0.9925	0.9845	0.9805	0.9734
	Multi	None	0.8786	0.9047	0.8644	0.7840	0.8398	0.7481
		Fuzzy	0.9014	0.9090	0.8976	0.8137	0.8576	0.7867
		Two-stage Cutout	0.9839	0.9944	0.9782	0.9612	0.9775	0.9653
		Above two	0.9770	0.9766	0.9772	0.9543	0.9653	0.9482
ROAD	Binary	None	0.8139	0.6658	0.8612	0.7283	0.6061	0.5411
		Fuzzy	0.8388	0.7125	0.8822	0.7953	0.6726	0.6117
		Two-stage Cutout	0.9225	0.8621	0.9434	0.8876	0.8627	0.8187
		Above two	0.9326	0.8853	0.9517	0.8951	0.8850	0.8422
	Multi	None	0.7302	0.9910	0.0437	0.7318	0.8419	0.1057
		Fuzzy	0.7394	0.9706	0.1198	0.7497	0.8447	0.1455
		Two-stage Cutout	0.8569	0.9778	0.5341	0.8515	0.9093	0.6179
		Above two	0.8874	0.9167	0.8106	0.9289	0.9217	0.7253

removing the 0 and 255 pixels because they contain too many pixels, so the distribution of other pixels cannot be well reflected.

Following the processing of the data, it becomes evident that high and low signals (black and white parts in the picture) have been distributed differently. Furthermore, the gray distribution of these pixels is not uniform, but aggregation centers are more numerous. Using fuzzy theory, lesion information is implicitly labeled in an image through pixel clustering. According to theory, as long as the homologous data is present, the method should be effective, so it may be suitable for migration purposes.

3.2. The Binary and Multi-Classification results on two datasets with different enhancement modules

The results of binary and multi classification on these two datasets are summarized in Table 1. All models will perform better when two-stage cutouts are incorporated. KACD models' performance virtually declines with fuzzy; however, road models' performance increases slightly with fuzzy applied to the road dataset. There is a great deal of similarity in the internal structure of the same organism as seen in the medical image. During the cutout process, part of an image is randomly deleted. Despite not destroying the overall characteristics of the target structure for medical images, this random deletion allows the neural network to gain a better understanding of the global information contained in the whole image, which is equivalent to allowing the network to observe an image from a variety of angles. As a result, after using cutout, both data sets will be classified more accurately. In addition to processing the image, the FCM algorithm identifies the key areas of the image, which is equivalent to selecting features. KACD contains only a single image with a limited number of features. In this way, some features that contain important details may also be filtered out after a wide range of feature filtering. The ROAD dataset, however, contains multiple layers of sliced data, including a more extensive set of features. Although the method may inadvertently eliminate some features with desirable attributes, it still yields an overall improvement as it

Table 2
Classification results with different existing methods

Dataset	Type	Modules	ACC	SN	SP	PR	F1 Score	MCC
KACD	Binary	Conformer	0.7060	0.7061	0.7061	0.7174	0.7022	0.4233
		ConvNext	0.5403	0.2645	0.8156	0.5889	0.3650	0.0960
		Resnest50	0.5004	1.0000	0.0016	0.5000	0.6667	0.0280
		Resnet18	0.6873	0.6495	0.7250	0.7022	0.6748	0.3755
		Seresnet50	0.6857	0.7731	0.5984	0.6578	0.7108	0.3773
		ShuffleNet	0.8038	0.8028	0.8047	0.8041	0.8034	0.6075
		Swin Transformer	0.7381	0.7527	0.7234	0.7310	0.7417	0.4764
		T2T	0.5809	0.9390	0.2234	0.5469	0.6912	0.2324
		Vit	0.6912	0.8059	0.5766	0.6552	0.7228	0.3930
		Proposed Method	0.9898	0.9772	0.9925	0.9845	0.9805	0.9734
	Multi	Conformer	0.7866	0.3741	0.8203	0.4721	0.3854	0.2304
		ConvNext	0.7514	0.2728	0.7512	0.8754	0.2094	0.1108
		Resnest50	0.7740	0.3283	0.7988	0.7602	0.3220	0.1964
		Resnet18	0.7678	0.3051	0.7773	0.7549	0.2862	0.1699
		Seresnet50	0.7643	0.3212	0.7943	0.7552	0.3165	0.1825
		ShuffleNet	0.8628	0.5843	0.8905	0.6029	0.5782	0.4800
		Swin Transformer	0.8206	0.4124	0.8431	0.7303	0.4287	0.3391
		T2T	0.7514	0.2728	0.7513	0.7505	0.2094	0.1057
		Vit	0.7787	0.3582	0.8154	0.7859	0.3579	0.2615
		Proposed Method	0.9770	0.9766	0.9772	0.9543	0.9653	0.9482
ROAD	Binary	Conformer	0.6943	0.9030	0.4859	0.6369	0.7469	0.4278
		ConvNext	0.5246	0.0892	0.9594	0.6867	0.1579	0.0986
		Resnest50	0.6286	0.3631	0.8938	0.7733	0.4941	0.3030
		Resnet18	0.6818	0.6056	0.7578	0.7140	0.6554	0.3677
		Seresnet50	0.6896	0.7074	0.6719	0.6828	0.6949	0.3795
		ShuffleNet	0.7686	0.9061	0.6313	0.7104	0.7964	0.5588
		Swin Transformer	0.7833	0.9957	0.0588	0.7831	0.8767	0.1783
		T2T	0.5371	0.1581	0.9156	0.6516	0.2544	0.1129
		Vit	0.6763	0.8372	0.5156	0.6331	0.7210	0.3726
		Proposed Method	0.9326	0.8853	0.9517	0.8951	0.8850	0.8422
	Multi	Conformer	0.7128	0.4470	0.7505	0.6999	0.4333	0.2530
		ConvNext	0.6039	0.3591	0.6716	0.4713	0.3372	0.0654
		Resnest50	0.7319	0.5041	0.7727	0.8350	0.4541	0.3736
		Resnet18	0.7191	0.4510	0.7523	0.7025	0.4367	0.2607
		Seresnet50	0.6982	0.4780	0.7646	0.5656	0.4537	0.2830
		ShuffleNet	0.8156	0.6773	0.8474	0.6954	0.6848	0.5337
		Swin Transformer	0.8533	0.6765	0.8995	0.8503	0.5892	0.5906
		T2T	0.6717	0.3570	0.6861	0.3788	0.3016	0.0699
		Vit	0.6998	0.4347	0.7506	0.4262	0.3990	0.1840
		Proposed Method	0.8874	0.9167	0.8106	0.9289	0.9217	0.7253

effectively filters out a substantial number of redundant or interfering features.

3.3. Performance compared with existing methods

A comparison was also made with other advanced methods [34–42], enough iterations are used to satisfy the fitness value, and the random 5-fold cross-validation is used to evaluate the performance. The evaluation system is incapable of guaranteeing that all indicators of one model are greater than those of other models. As the most important indicators for biomedical image classification, ACC, F1-score, and MCC are used here as the three criteria for model selection.

The experimental results demonstrate that the proposed method excels in various scenarios, including both datasets and diverse classification tasks. The method's performance in ACC, F1-score, and MCC is remarkable, particularly in the KACD dataset. As shown in Table 2, in binary classification, the method achieves an accuracy of 98%, while in multi-classification, it reaches 97%, outperforming most other methods. The performance gap between the proposed method and other models in the ROAD data is not substantial, likely due to the smaller number of images in the ROAD dataset compared to KACD. Therefore, the full potential of the method is not realized. Nevertheless, upon addressing these limitations, there is potential for further improvement, positioning the proposed method as more efficient than other mainstream approaches.

3.4. Running environment and training time with different enhancement Modules

The experiments were performed on a computing server equipped with an Intel i9-11900 K CPU, NVIDIA RTX-3090 GPU, and Kingston 32 GB memory. On the server, Ubuntu 18.04 was running. It used Python version 3.8 and Torch version 1.10.0. The learning rate was 5×10^{-4} and the batch size was 64. Fig. 4 shows the time required to train an epoch. Using FCM, the training time has been reduced, especially in the ROAD dataset, where it has reduced running speed by more than 20%.

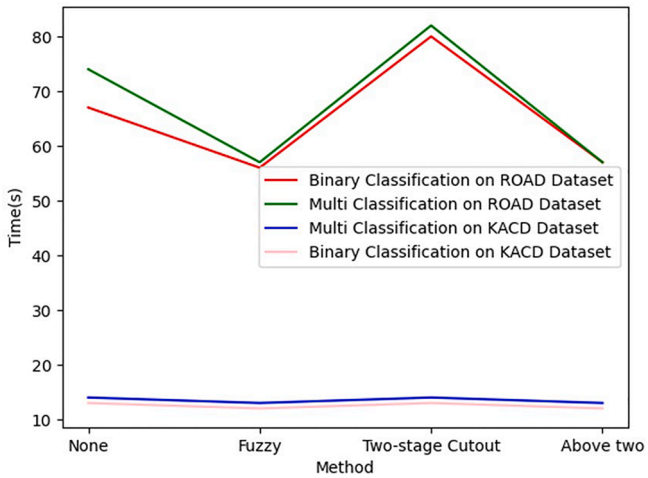

Fig. 4. Training time with Different Enhancement Modules.

3.5. Potential practical applications

The fact that medical image information involves patient privacy requires ensuring data security in scientific research and making sure it cannot be used by lawbreakers. Blockchain technology represents a peer-to-peer developed public ledger that is the foundation of bitcoin, and has slowly gained attention since 2008 [43,44]. As part of the ledger, newly generated transaction data will be encrypted, packaged as a data block, then connected to the end of the chain table. This is a chain table consisting of blocks arranged chronologically. Blockchains feature decentralization, unforgeability, transparency, traceability, and the capability to support a wide range of applications, such as smart contracts. This endows them with excellent data security and privacy capabilities [45,46]. The following three main characteristics, we believe, distinguish a model with high portability to blockchain technology: the model can transition quickly between various tasks, resulting in little fine tuning required, and it has high recognition accuracy after migration. Finally, the model is robust to a wide variety of tasks. The proposed method can be combined with current popular blockchain technology. This will enable us to take advantage of its distributed and decentralized characteristics to achieve data preprocessing in hospital data centers and training on cloud servers. It is not only possible to make efficient use of data, but it is also possible to ensure its security. Meanwhile, this method is simple to implement, can be integrated with blockchain technology, and is feasible.

4. Conclusion

This study aims to develop a deep learning method for predicting Alzheimer's disease stages based on brain MRI. The image is first processed using the FCM method. Thus, local features of the image that contain significant information are revealed. In this way, the algorithm becomes more efficient and the results are more accurate. To further improve performance, the cutout method was applied. Randomly cutting up the image can help the neural network identify the global information contained therein. The experiment shows that the fuzzy VGG model is more efficient than other methods on all performance evaluation indicators. Future studies will use the image dataset collated internally for analysis and combine it with other information from other electronic medical records of patients to conduct further imageomics research.

5. Funding statement

This work was supported by the Key Research and Development Program of Liaoning Provence. (2019JH2/10300010), as well as Liaoning Province Applied Basic Research Program (Joint Plan) Project (2022JH2/101500021).

6. Data availability statement

The data used to support the findings of this study are included in the article.

Declaration of Competing Interest

The authors declare that they have no known competing financial interests or personal relationships that could have appeared to influence the work reported in this paper.

Data availability

The authors do not have permission to share data.

Appendix A. Supplementary data

Supplementary data to this article can be found online at https://doi.org/10.1016/j.ins.2023.119129.

References

[1] R.E. Tanzi, L. Bertram, Alzheimer's disease: The latest suspect, Nature 454 (2008) 706–708.
[2] Anonymous, 2021 Alzheimer's disease facts and figures, Alzheimer's & Dementia, 17 (2021).
[3] A. Akomolafe, A. Beiser, J.B. Meigs, R. Au, R.C. Green, L.A. Farrer, P.A. Wolf, S. Seshadri, Diabetes Mellitus and Risk of Developing Alzheimer Disease: Results From the Framingham Study, Arch. Neurol. 1 (2006) S26–S27.
[4] A. Alzheimer, Uber eine eigenartige Erkrankung der Hirnride, Allg.z.psychiatr, (1907).
[5] W.-D. Bao, P. Pang, X.-T. Zhou, F. Hu, W. Xiong, K. Chen, J. Wang, F. Wang, D. Xie, Y. Hu, Z.-T. Han, H.-H. Zhang, W.-X. Wang, P.T. Nelson, J.-G. Chen, Y. Lu, H.-Y. Man, D. Liu, L.-Q. Zhu, Loss of ferroportin induces memory impairment by promoting ferroptosis in Alzheimer's disease, Cell Death Differ. 28 (2021) 1548–1562.
[6] Z.S. Khachaturian, of Alzheimer's disease, Arch. Neurol. 42 (11) (1985) 1097–1105.
[7] N. Falgàs, C.M. Walsh, T.C. Neylan, L.T. Grinberg, Deepen into sleep and wake patterns across Alzheimer's disease phenotypes, Alzheimers Dement. 17 (8) (2021) 1403–1406.
[8] None, Automated MRI measurements accurately identify clinically probable Alzheimer's disease, Nature Clinical Practice Neurology, 3 (2007) 124-124.
[9] T. Li, Z.-l. Liao, Y.-p. Mao, J.-j. Hu, D. Le, Y. Pei, W. Sun, J. Lin, Y.-j. Qiu, J.-p. Zhu, Y. Chen, C. Qi, X. Ye, H. Su, E. Yu, Temporal dynamic changes of intrinsic brain activity in Alzheimer's disease and mild cognitive impairment patients: a resting-state functional magnetic resonance imaging study, Annals of Translational Medicine, 9 (2021).
[10] G. Battineni, N. Chintalapudi, F. Amenta, E. Traini, A Comprehensive Machine-Learning Model Applied to Magnetic Resonance Imaging (MRI) to Predict Alzheimer's Disease (AD) in Older Subjects, J. Clin. Med. 9 (2020) 1–14.
[11] M. Agarwal, L. Saba, S.K. Gupta, A.M. Johri, N.N. Khanna, S.I. Mavrogeni, J.R. Laird, G. Pareek, M. Miner, P.P. Sfikakis, A.D. Protogerou, A.M. Sharma, V. Viswanathan, G.D. Kitas, A.N. Nicolaides, J.S. Suri, Wilson disease tissue classification and characterization using seven artificial intelligence models embedded with 3D optimization paradigm on a weak training brain magnetic resonance imaging datasets: a supercomputer application, Med. Biol. Eng. Compu. 59 (3) (2021) 511–533.
[12] J. Whitwell, D. Dickson, M. Murray, R. Petersen, C. Jack, K. Josephs, Neuroimaging Correlates of Pathologically-Defined Atypical Alzheimer's Disease (P05. 049), in, AAN Enterprises, 2012.
[13] C.M. Dartora, A. Marseglia, G. Mårtensson, G. Rukh, J. Dang, J.-S. Muehlboeck, L.-O. Wahlund, R. Moreno, J. Barroso, D. Ferreira, H. Schiòlth, E. Westman, A.s. D.N. Initiative, A.I.B. flagsh, Lifestyle, J.A.s.D.N. Initiati, A. consortium, Predicting the Age of the Brain with Minimally Processed T1-weighted MRI Data, in: medRxiv, 2022.
[14] J. Venugopalan, L. Tong, H. Hassanzadeh, M.D. Wang, Multimodal deep learning models for early detection of Alzheimer's disease stage, Sci. Rep. 11 (2021).
[15] Z. Yang, I.M. Nasrallah, H. Shou, J. Wen, J. Doshi, M. Habes, G. Erus, A. Abdulkadir, S.M. Resnick, D.A. Wolk, C. Davatzikos, Disentangling brain heterogeneity via semi-supervised deep-learning and MRI: Application to dimensional representations of Alzheimer's disease, Alzheimers Dement. 17 (2021).
[16] Y. Eroğlu, M. Yildirim, A.C. Cinar, mRMR-based hybrid convolutional neural network model for classification of Alzheimer's disease on brain magnetic resonance images, Int. J. Imaging Syst. Technol. 32 (2021) 517–527.
[17] L. Sathish Kumar, S. Hariharasitaraman, K. Narayanasamy, K. Thinakaran, J. Mahalakshmi, V. Pandimurugan, AlexNet approach for early stage Alzheimer's disease detection from MRI brain images, Mater. Today:. Proc. 51 (2022) 58–65.
[18] Z. Fan, J. Li, L. Zhang, G. Zhu, P. Li, X. Lu, P. Shen, S.A.A. Shah, T. Bennamoun, W.W. Hua, U-net based analysis of MRI for Alzheimer's disease diagnosis, Neural Comput. & Applic. 33 (2021) 13587–13599.
[19] M. Liu, J. Zhang, E. Adeli, D. Shen, Landmark-based deep multi-instance learning for brain disease diagnosis, Med. Image Anal. 43 (2018) 157–168.
[20] C.L. Saratxaga, I. Moya, A. Picón, M. Acosta, A. Moreno-Fernandez-de-Leceta, E. Garrote, A. Bereciartua-Perez, MRI Deep Learning-Based Solution for Alzheimer's Disease Prediction, J. Personalized Med. 11 (9) (2021) 902.
[21] A. Mehmood, S. Yang, A.A.L. Smadi, M. Yaqub, A Transfer Learning Approach for Early Diagnosis of Alzheimer's Disease on MRI Images, Neuroscience 460 (2021) 43–52.
[22] F.E.K. Al-Khuzaie, O. Bayat, A.D. Duru, M.Y. Alzahrani, Diagnosis of Alzheimer Disease Using 2D MRI Slices by Convolutional Neural Network, Appl. Bionics Biomech. 2021 (2021) 1–9.
[23] W. Lin, W. Lin, G. Chen, H. Zhang, Q. Gao, Y. Huang, T. Tong, M. Du, Bidirectional Mapping of Brain MRI and PET With 3D Reversible GAN for the Diagnosis of Alzheimer's Disease, Front. Neurosci. 15 (2021).
[24] B. Mallikarjuna, G. Shrivastava, M. Sharma, Blockchain technology: A DNN token-based approach in healthcare and COVID-19 to generate extracted data, Expert. Syst. 39 (2021).
[25] T. DeVries, G.W. Taylor, Improved regularization of convolutional neural networks with cutout, arXiv preprint arXiv:1708.04552, (2017).
[26] Dubey S. Alzheimer's Dataset, in.
[27] CCF BDCI Recognition of Alzheimer's Disease Dataset, in.
[28] I. Borlea, R.E. Precup, A.-B. Borlea, D.T. Iercan, A Unified Form of Fuzzy C-Means and K-Means algorithms and its Partitional Implementation, Knowl. Based Syst. 214 (2021), 106731.
[29] S. Askari, Fuzzy C-Means clustering algorithm for data with unequal cluster sizes and contaminated with noise and outliers: Review and development, Expert Syst. Appl. 165 (2021) 113856.
[30] PP.Y. Muddappa, T. Rajanna, G. Giridhara, Effects of different interlaminar hybridization and cutout sizes on the vibration and buckling characteristics of fiber metal composite laminates under partial edge loads, Proc. Inst. Mech. Eng., Part C: J. Mech. Eng. Sci. 236 (2) (2022) 1083–1098.
[31] A Model-Agnostic Derivative of Cutout for Image Data Augmentation, in, 2022.
[32] L. Tang, Image Classification Based On improved VGG Network, 2021 IEEE 6th International Conference on Signal and Image Processing (ICSIP), (2021) 316-320.
[33] X. Wang, C. Dong, Y. Shan, RepSR: Training Efficient VGG-style Super-Resolution Networks with Structural Re-Parameterization and Batch Normalization, Proceedings of the 30th ACM International Conference on Multimedia, (2022).
[34] Z. Peng, W. Huang, S. Gu, L. Xie, Y. Wang, J. Jiao, Q. Ye, Conformer: Local Features Coupling Global Representations for Visual Recognition, 2021 IEEE/CVF International Conference on Computer Vision (ICCV), (2021) 357-366.

[35] Z. Liu, H. Mao, C. Wu, C. Feichtenhofer, T. Darrell, S. Xie, A ConvNet for the 2020s, 2022 IEEE/CVF Conference on Computer Vision and Pattern Recognition (CVPR), (2022) 11966-11976.
[36] H. Zhang, C. Wu, Z. Zhang, Y. Zhu, Z.-L. Zhang, H. Lin, Y. Sun, T. He, J. Mueller, R. Manmatha, M. Li, A. Smola, ResNeSt: Split-Attention Networks, 2022 IEEE/CVF Conference on Computer Vision and Pattern Recognition Workshops (CVPRW), (2020) 2735-2745.
[37] K. He, X. Zhang, S. Ren, J. Sun, Deep Residual Learning for Image Recognition, 2016 IEEE Conference on Computer Vision and Pattern Recognition (CVPR), (2015) 770-778.
[38] J. Hu, L. Shen, S. Albanie, G. Sun, E. Wu, Squeeze-and-Excitation Networks, IEEE Trans. Pattern Anal. Mach. Intell. 42 (2017) 2011–2023.
[39] X. Zhang, X. Zhou, M. Lin, J. Sun, ShuffleNet: An Extremely Efficient Convolutional Neural Network for Mobile Devices, 2018 IEEE/CVF Conference on Computer Vision and Pattern Recognition, (2017) 6848-6856.
[40] Z. Liu, Y. Lin, Y. Cao, H. Hu, Y. Wei, Z. Zhang, S. Lin, B. Guo, Swin Transformer: Hierarchical Vision Transformer using Shifted Windows, 2021 IEEE/CVF International Conference on Computer Vision (ICCV), (2021) 9992-10002.
[41] L. Yuan, Y. Chen, T. Wang, W. Yu, Y. Shi, F.E.H. Tay, J. Feng, S. Yan, Tokens-to-Token ViT: Training Vision Transformers from Scratch on ImageNet, 2021 IEEE/CVF International Conference on Computer Vision (ICCV), (2021) 538-547.
[42] A. Dosovitskiy, L. Beyer, A. Kolesnikov, D. Weissenborn, X. Zhai, T. Unterthiner, M. Dehghani, M. Minderer, G. Heigold, S. Gelly, J. Uszkoreit, N. Houlsby, An Image is Worth 16x16 Words: Transformers for Image Recognition at Scale, ArXiv, abs/2010.11929 (2020).
[43] S. Nakamoto, Bitcoin: A Peer-to-Peer Electronic Cash System, in, 2008.
[44] A.S.V. Koe, S. Ai, P. Huang, A. Yan, J. Tang, Q. Chen, K. Mo, W. Jie, S. Zhang, Sender anonymity: Applying ring signature in gateway-based blockchain for IoT is not enough, Inf. Sci. 606 (2022) 60–71.
[45] C.C. Agbo, Q.H. Mahmoud, J.M. Eklund, Blockchain Technology in Healthcare: A Systematic Review, Healthcare 7 (2019).
[46] Z. Qu, Z. Zhang, M. Zheng, A quantum blockchain-enabled framework for secure private electronic medical records in Internet of Medical Things, Inf. Sci. 612 (2022) 942–958.